Ferroelectrics, 1991, Vol. 118, pp. 379–409
Reprints available directly from the publisher
Photocopying permitted by license only

PYROELECTRIC SENSORS FOR THE PHOTOTHERMAL ANALYSIS OF CONDENSED PHASES

H. COUFAL
IBM Research Division, Almaden Research Center, 650 Harry Road, San Jose, CA 95120-6099, USA

and

A. MANDELIS
Photoacoustic and Photothermal Sciences Laboratory, Department of Mechanical Engineering, and Ontario Laser and Lightwave Research Center, University of Toronto, Toronto, ON, M5S 1A4, Canada

(Received May 21, 1990)

The use of pyroelectric sensors for the detection of radiation induced thermal wave phenomena (the photopyroelectric effect) is reviewed. These sensors are compatible with most media—UHV, air, most liquids and solids—and have the potential for picosecond time resolution combined with a tremendous sensitivity. At first the signal generation process in such a sensor is briefly described and the importance of the ferroelectric material properties highlighted. The use of these devices as detectors of radiation-induced heating is then discussed in the time-resolved, and frequency-domain modes of excitation and detection and in a variety of spectral regions from radio waves to X-rays, electrons, ions and neutral particles. Condensed phase applications emphasizing the versatility and the unique properties of these detection schemes, as well as their inherent limitations will be presented. Typical applications in the thermal analysis and spectroscopy of thin films and the non-destructive evaluation of electronic materials are reviewed. Recent developments and future needs are finally discussed.

1. INTRODUCTION

Exposure of a sample to any form of radiation causes local heating via absorption and subsequent thermalization of energy. If the incident radiation is modulated or pulsed, a transient heat source is generated in the sample. Thermal waves and, due to thermal expansion, acoustic waves are launched into the sample under study and interact with the sample before being detected by one of the numerous detection schemes available nowadays.[1–4] This radiation induced heating is detected with acoustic transducers, whence the name photoacoustic (PA), or by other detection schemes, such as radiometry or laser beam deflection. In the latter case the technique is frequently referred to as photothermal (PT) even when electrons, ions or neutral particles are used for excitation. These PA and PT methods are ideal for the spectroscopic or thermal analysis of thin films, surfaces, and bulk materials.

Among the detection schemes, a recently developed pyroelectric sensor[5–8] combines, in an unique way, extreme sensitivity (10 pJ) with highest possible time resolution (100 ps) at low cost ($0.10). This detector has been utilized for a large number of applications over a wide temperature (16K–400K) and pressure ($(10^{-13}$

bar-30 bar) range in solid[5,6] gaseous as well as in liquid media.[9,10] In the following sections, the signal generation as well as the detection process with pyroelectric sensors of this type are briefly described. Particular emphasis is put on the dramatic influence of external detection electronics on the observed signals and the various photopyroelectric detection schemes. Design considerations and various available electret materials are then analyzed. After a discussion of the operating characteristics of these sensors, examples highlighting the versatility and the unique properties of this detection scheme are discussed. Finally, recent applications of electret sensors in the thermal analysis and spectroscopy of wide ranges of condensed phase materials are reviewed.

2. SIGNAL GENERATION AND DETECTION

The most convenient way to discuss the observed effects[11] is to describe the electret sensor by its pyroelectric coefficient $p(z, t)$, where z and t describe the depth and temporal dependence, respectively; sample and sensor are assumed to be homogeneous in the x and y directions. A change $\Theta(z, t)$ of the temperature distribution in the electret, relative to a reference temperature distribution, $T_0(z, t_0)$,

$$\Theta(z, t) = T(z, t) - T_0(z, t_0), \tag{1}$$

causes a change in polarization. In an electret film of thickness L, metallized on both faces, as shown in Figure 1, such a temperature change induces an electric charge $Q(t)$

$$Q(t) = \frac{1}{L}\int p(z, t)\Theta(z, t)\, dz \tag{2}$$

on the electrodes. An appreciable time dependence of the pyroelectric coefficient is only observed for large temperature variations or after long periods of time have elapsed. For the rest of the discussion we will, therefore, assume that the pyroelectric coefficient is not time dependent on the scale of the experiment. The observed charge $Q(t)$ is then proportional to the overlap integral of the temperature

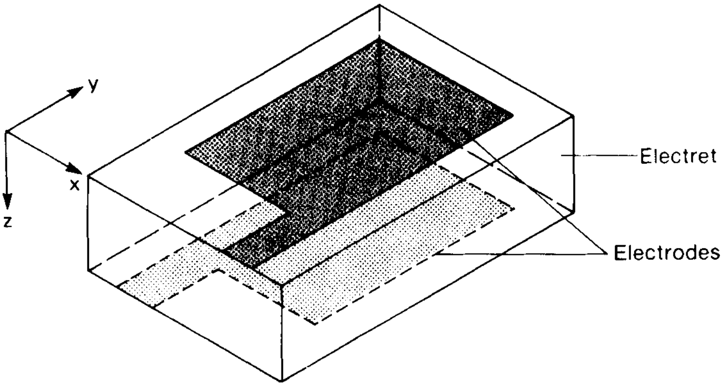

FIGURE 1 Schematic of pyroelectric sensor element with face-on electrodes.

distribution $\Theta(z, t)$ with the polarization profile $p(z)$. Two types of polarization profiles are of particular interest and greatly simplify the discussion of Equation 2.[8] The first one is an electret that has a surface charge or polarization, but is otherwise unpoled, the second one is a sensor which has a completely homogeneous polarization.

For an unpoled film with an electrical charge at the surface of the electret at $z = 0$ it can be shown that[8]:

$$Q(t) = \frac{\Theta(0, t)}{L}. \tag{3}$$

The induced charge is proportional to the temperature at the surface of the sample, and the electret can be used as a *thermometer* for surface temperatures. By poling a well-defined layer within an electret obviously the temperature at that depth can be probed. A homogeneously poled film can, of course, be described as a superposition of narrow polarization profiles. Selected depths can then be probed by narrow electrodes at the edge of the sensor.[12]

For homogeneous polarization the pyroelectric coefficient p is a constant. The observed charge is then proportional to the average temperature change in the film. The change $\Theta(z, t)$ of the temperature distribution in (1) is associated with a change $\Delta(t)$ in the heat content of the electret film, so that, assuming that the material parameters are temperature independent, and that the pyroelectric material is homogeneous, the induced charge is proportional to $\Delta(t)$:

$$Q(t) = \frac{p}{c\rho L}\,\Delta(t). \tag{4}$$

If heat loss from the pyroelectric element into the surroundings can be neglected, the element is in fact a pyroelectric *calorimeter*. This condition can be met, for example, by placing a thin sample on a large, self supporting piece of pyroelectric foil. The time resolution of the detector itself is only limited by the time required to convert an input of thermal energy into a change of polarization, a process that can take place in femtoseconds. The time resolution of the complete sample-detector assembly is then only limited by the thermal propagation time τ_t from the sample surface to the interface with the detector. The temperature at a given distance ℓ from a pulsed heat source reaches its maximum at a time τ_t after the excitation. For one-dimensional heat flow the thermal transit time τ_t is determined by[13]

$$\tau_t = \frac{\ell^2}{6\beta}, \tag{5}$$

where β is the thermal diffusivity of the sample. With a suitable thin film sample directly deposited onto one of the electrodes of the detector, a time resolution of the order of hundred picoseconds can be achieved.[8] With such a sample, essentially all the energy absorbed by the sample will diffuse into the detector, resulting in the largest possible signal. This pyroelectric calorimeter is, therefore, the detector with the best signal/noise ratio of all thermal detection schemes. The time resolution of the sample/detector combination is independent from the temperature distribution in the calorimeter and limited only by thermal diffusion from the sample across the interface to the calorimeter. The pyroelectric calorimeter, directly attached to a sample, has therefore the highest possible time resolution of all thermal detectors. This combination of sensitivity and time resolution in one sensor is a unique feature of the pyroelectric calorimeter making it the prime choice for photothermal analysis of thin films.

The signal of the pyroelectric calorimeter is proportional to the average temperature change in the device. If thermal equilibrium is reached between the sample and the calorimeter and within the calorimeter, the observed signal is proportional to the sample temperature. The relative magnitude of the thermal transit time across the sample according to (5) and the thermal transit time across the calorimeter, derived by using calorimeter properties in (5), determines in this case the overall time resolution. For a calorimeter with a thickness of μm the time resolution as a thin film thermometer will be on the order of μs.

Heat transport is governed by temperature gradients. Heat flow from a heated source, the sample, to a cold heat sink, the calorimeter, is therefore proportional to the sample temperature. After the excitation pulse, the heat flow from the sample into the calorimeter will initially be proportional to the sample temperature and the calorimeter can serve as an ultrafast thermometer. These arguments are supported by an extensive computer simulation of the signal generation process. This simulation showed that the electrical signal from a pyroelectric calorimeter is proportional to the surface temperature of the sample during and immediately after a short excitation pulse and once sample and calorimeter are in thermal equilibrium.[14]

With frequency dependent studies being extremely popular for applications, such as depth profiling or thermal diffusivity measurements, a detailed general one-dimensional photopyroelectric theory has been developed to account in a quantitative fashion for experimental observations of optical and thermal effects in the frequency-domain.[15] Simplified specialized models have also been developed to account for thermal property measurements using the photopyroelectric effect.[16–18] These specialized models are, in principle, special cases of the more general theory by Mandelis and Zver,[15] whose main features are discussed below.

A one-dimensional geometry of a photopyroelectric system is shown in Figure 2. A solid sample, of thickness L_s, is irradiated by monochromatic light of wave-

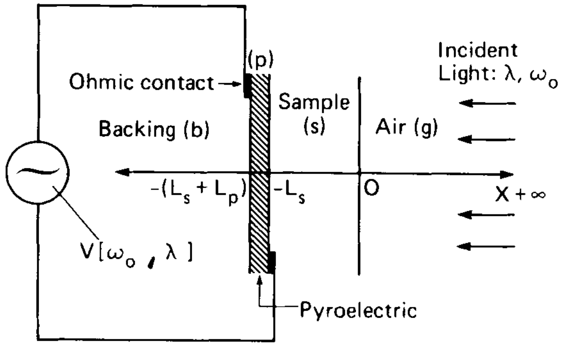

FIGURE 2 One-dimensional geometry of a frequency-domain photopyroelectric system. See text for details.[15]

length λ, whose intensity is modulated at angular frequency ω_0 by a chopper. The sample has optical absorption coefficient $\alpha_s(\lambda)$ and is in intimate contact with a pyroelectric transducer thin film of thickness ℓ. The optical absorption coefficient and pyroelectric coefficient of the detector are $\alpha_p(\lambda)$ and p, respectively. The sample/transducer system is supported by a transparent backing material of thickness large, compared to L_s or ℓ. The photopyroelectric cell, unlike the photoacoustic cell, does not require hermetic closure (open geometry), and the incident light is assumed to illuminate the sample surface uniformly. Light absorption by the sample/transducer system and nonradiative energy conversion to heat increases the temperature of the pyroelectric thin film. This temperature increase results in a potential difference between the upper and lower surfaces of the transducer due to the pyroelectric effect. This voltage $V[\omega_0, \alpha_s(\lambda)]$ amounts to an electric signal, which is measured in the external circuit through the connection of Ohmic leads to the pyroelectric as shown in Figure 2.

The charge accumulated in the pyroelectric, due to a change $\Theta(t)$ in temperature is given by

$$q(t) = p\Theta(t). \tag{6}$$

For a thin pyroelectric film of thickness ℓ, exposed to a sinusoidally varying temperature field, the average ac pyroelectric voltage under no load conditions is given by

$$V(\omega_0) = \left[\frac{P\ell\theta_p(\omega_0)}{K\varepsilon_0}\right] \exp(i\omega_0 t) \tag{7}$$

where

$$\theta_p(\omega_0) \equiv \frac{1}{\ell}\int_{\text{Thickness},\ell} \Theta_p(\omega_0, x)\, dx, \tag{8}$$

K is the pyroelectric sensor dielectric constant, and ε_0 is the permitivity constant of vacuum (8.85418×10^{12} $C/V-m$). $\Theta(\omega_0, x)$ is the ac temperature field in the bulk of the pyroelectric, a result of heat conduction processes through the radiation absorbing solid. For the geometry of Figure 2 the field $\Theta(\omega_0, x)$ can be found from the solution of coupled, one-dimensional thermal transport equations. Allowing for the finite optical absorption coefficients α_s and α_p, and assuming negligible optical reflection and radiative heat transfer coefficients on the sample surface and pyroelectric-sample interface,[19] the appropriate heat diffusion equations have been solved, coupled via boundary conditions of temperature and heat flux continuity at all interfaces.

The resulting full expression for the film-thickness-averaged photopyroelectric voltage has been evaluated numerically for the amplitude $|V(\omega_0)|$ and phase $\Phi(\omega_0)$ of the signal. The following numerical values were used for these calculations: $I_0 = 1$ W/m^2. $p = 3 \times 10^{-5}$ C/m^2-°K, $K = 12$, $\varepsilon_0 = 8.854 \times 10^{-12}$ $C/V-m$, $\ell = 28$ μm, $\beta_p = 5.4 \times 10^{-8}$ m^2/sec, $k_p = 0.13$ W/m-°K, $k_g = 2.38 \times 10^{-2}$ W/m-°K, $\beta_g = 1.9 \times 10^{-5}$ m^2/sec (g = air), and $L_s = 50$ μm. All other parameters were allowed to vary.

The values for p, K, ℓ, β_p and k_p were obtained from the Kynar™ Piezo Film Technical Manual, Pennwalt Corp., King of Prussia, Penn.[20]

Figure 3A shows the theoretical spectral response to a Gaussian absorption band centered at 500 nm, with the chopping frequency as a parameter. A spectral inversion of the absorption amplitude peak at higher frequencies is observed, due to the interplay in thermal energy contribution between the sample and the pyroelectric. No inversion occurs in the phase data, which correlates with the amplitude for $f < 20$ Hz, and anticorrelates with it for higher frequencies. These calculations show that the photopyroelectric voltage is governed by the interplay between optical absorption in the sample and thermal response of the pyroelectric transducer. Figure 3B shows experimental results demonstrating the spectroscopic nature of the photopyroelectric detection in the thermally thin limit and verification of the spectral inversion features predicted by the frequency-domain theory.[6,16]

3. INSTRUMENTATION AND MEASUREMENT

Pyroelectric elements have been utilized in photothermal analysis in three basic experimental configurations, depending on signal generation and detection mode: pulsed optical excitation of the sample and pyroelectric calorimetric detection (time-domain scheme); harmonic modulation of the irradiance of the optical source at a single frequency, and pyroelectric thermometric or calorimetric detection (frequency-domain scheme); and frequency multiplexed excitation, followed by correlation and spectral analysis of input and output signal channels. This latter scheme involves a group of techniques, which may be viewed as intermediate between time- and frequency-domain photopyroelectric detection.

3.1. Time Domain Instrumentation

Early instrumentation for the pyroelectric detection of transient optical heating involved pulsing pyroelectric materials serving as samples ($BaMnF_4$ and $Sr_xBa_{1-x}Nb_2O_6$),[21,22] as well as actual opaque thin samples (e.g., nichrome-coated Mylar)[23] bonded on a pyroelectric transducer, with ms to ns-duration laser pulses. Those measurements were geared toward the determination of thermal diffusivities and pyroelectric coefficients. Relatively thick pyroelectric transducers were used, typically of several mm thickness. The pyroelectric current response was measured, using the standard detector-amplifier resistive-capacitive equivalent circuit[23] shown in Figure 4 and time-domain solutions to the circuit equation[22]:

$$V(t) = e^{-t/\tau_E} \int_0^t dt' e^{t'/\tau_E} \frac{pA}{C_A + C_P} \frac{d}{dt'} \overline{\theta_p(t')} \tag{9}$$

where $\overline{\theta_P(t)}$ is the spatial average (with respect to the pyroelectric element thickness) of the temperature in the transducer, A is the active detector area, and τ_E is the electronic time constant of the element-preamplifier system:

$$\tau_E \equiv RC = \left(\frac{1}{R_A} + \frac{1}{R_P}\right)^{-1} (C_A + C_P) \simeq 68\ \mu\text{s} \tag{10}$$

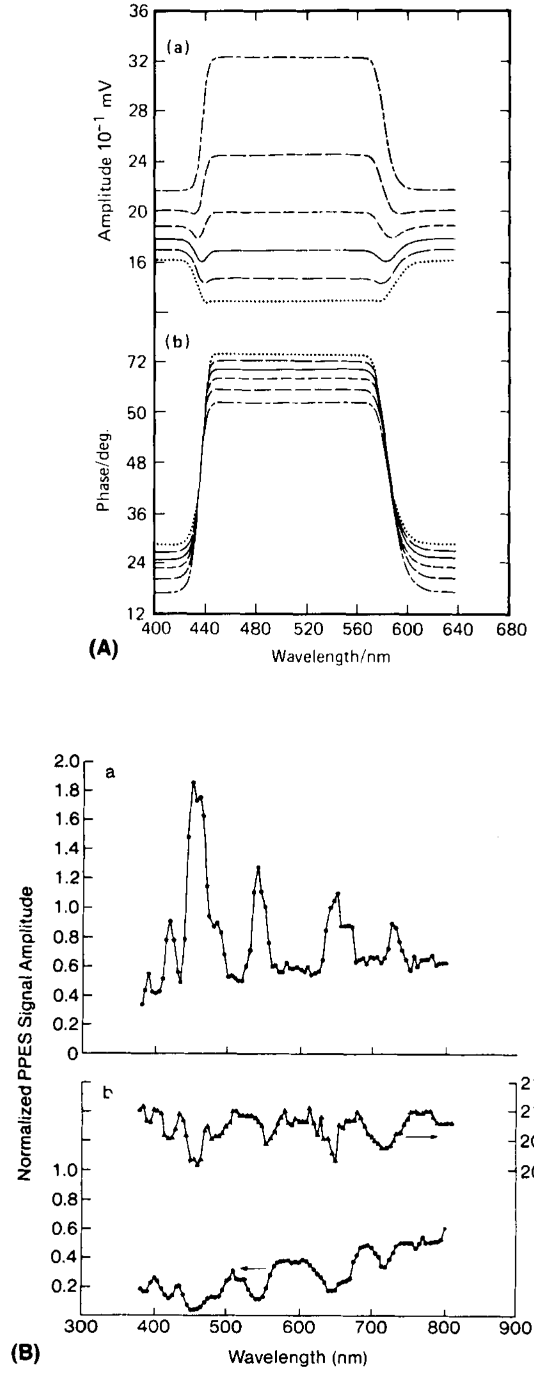

FIGURE 3 (A) Photopyroelectric spectroscopic response to a Gaussian absorption band with $0 \leq \alpha_s \leq 10^5$ cm^{-1} as a function of the light modulation frequency: a) Amplitude curves; from top to bottom: F = 10 Hz, 15 Hz, 20 Hz, 25 Hz, 30 Hz and 35 Hz, respectively; and b) Phase profiles corresponding to amplitude curves in (a).[15] (B) Photopyroelectric spectrum of Ho_2O_3 powder mixed with water. Chopping frequency 11 Hz (a); and 50 Hz (b). Notice spectral inversions in (b).[6]

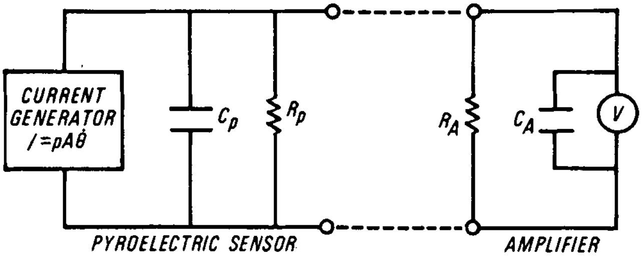

FIGURE 4 Equivalent electrical circuit of a pyroelectric detector and preamplifier.[11]

Due to the long observation time intervals usually involved with samples ($\gtrsim$ 1 ms) compared to τ_E, Equation (9) was simplified further:

$$V(t) \simeq pAR_A \frac{d}{dt}\overline{\theta_P(t)} \qquad (11)$$

Equation (11) can also be obtained as a special case of the more complete circuit theory by Coufal *et al.*[7] in the non-calorimetric temporal regime, a result of the thick-sample and slow-transducer combination typical of the early time-domain photopyroelectric instrumentation. It is worth mentioning that Byer and Roundy[21] were successful in time-resolving a Q-switched CO_2 laser pulse using a $Sr_xBa_{1-x}Nb_2O_6$ pyroelectric detector of 0.1 mm thickness with a 1 MΩ amplifier load resistor. This circuit was shown to resolve risetimes from 1 ms to 4 ns at a significant loss of responsivity, compared to a much slower detector connected to a 22 MΩ amplifier resistance. In general, if fast response to laser-induced radiation pulses is desired, pyroelectric elements with maximum flat transfer function must be used. This, in turn, requires minimum τ_E. Very short electrical time constant can be achieved by minimizing the pyroelectric element capacitance using an edge-electroded detector, and/or by minimizing the input impedance, R_A, of the amplifier.[23] This can only be done at the expense of reduced signal, Equation (11), and overall responsivity.

In order to achieve sub-microsecond time resolution in photopyroelectric detection several criteria must be met by the transducer.[10] The main requirements are: low specific heat for operation as an ideal calorimeter; mechanical flexibility in order to facilitate intimate thermal contact with sample; fast thermal equilibration accompanied by negligible lateral heat losses; a relatively large pyroelectric coefficient and a small dielectric constant, in order to achieve optimal signals. These criteria are largely met by thin β-PVDF pyroelectric films, readily available commercially in the μm-thickness range. Further requirements with respect to the sample geometry involve a thermally thin sample, with the time-dependent thermal diffusion length longer than the effective sample thickness,[24] $T - A(\lambda)$, on the time scale of the experiment. T and $A(\lambda)$ represent geometrical thickness and optical absorption length at excitation wavelength λ, respectively. This criterion stipulates the use of thin-film samples directly deposited on the pyroelectric transducer. Finally, specific conditions regarding the design of fast risetime high-impedance preamplifiers must be satisfied, as discussed below. Signal generation and detection instrumentation is readily available nowadays, in terms of ns- and sub-ns pulsed lasers and fast transient digitizers or boxcar analyzers for time-gated detection. Due to the above-mentioned criteria, most pulsed sub-μs time-resolved photopyroelectric work to-date has been performed using thin film samples deposited on β-PVDF calorimeters. A schematic of a typical photopyroelectric experimental set-up is shown in Figure 5.

3.2. *Frequency-Domain Instrumentation*

Frequency-domain photopyroelectric instrumentation has the virtue of being extremely simple, yielding high-quality signals with very inexpensive thin-film PVDF detectors, the detectivity of which is limited by Johnson noise.[25] Early work with optically and electrically heated, coated PVF or PVDF thin films (6–12 μm) established the inequivalence of response to these two excitation modes due to interference by the thermal properties of the black-body coating evaporated on the transducer to enhance absorptivity.[26] Significantly, the frequency-response analysis of pyroelectric signals from both types of thin films over wide frequency ranges 10^{-3}–10^{4} Hz) gave information about the substantial degree of polarization nonuniformity throughout the thickness of the polymeric films.[26] Despite recent technological achievements and progress toward higher grades of poling uniformity, several problems persist in this area.[27] Historically, the first experiments using laser-induced frequency-domain photopyroelectric detection were performed in attempts to characterize the transducer itself (a $Pb_5Ge_3O_{11}$ pyroelectric crystal).[28] PVDF-based pyroelectric sensors, however, were recognized fairly early as attractive choices for applications in situations demanding high detectivity coupled with a broad spectral response and large active areas.[29] Very recently, novel high-detectivity pyroelectric detectors based on a bilayer laminate of polymer film (pyroelectric bimorphs) have been used as photothermal transducers.[30] These devices were found to have a peak detectivity of 6.6×10^{8} cm $Hz^{1/2}W^{-1}$, twice that for a

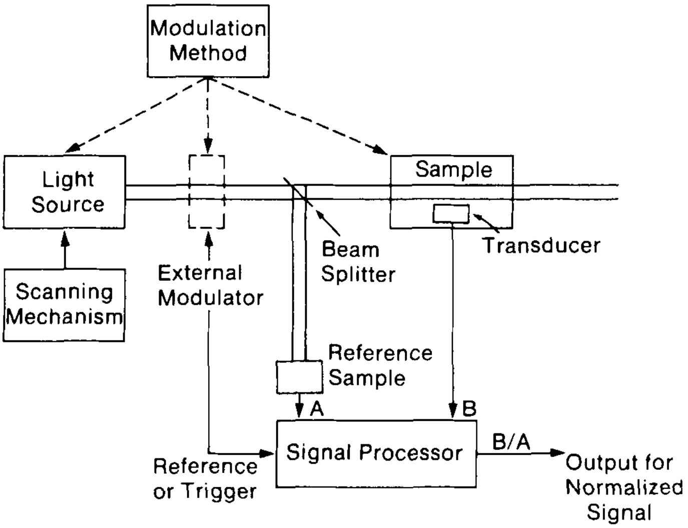

FIGURE 5 Generic pyroelectric photothermal instrumentation, including pulsed optical excitation and detection.

single-element PVDF detector. In terms of frequency-domain photopyroelectric signal acquisition and processing instrumentation, conventional apparatus may be used (Figure 6).[6] One advantage of the photopyroelectric frequency response over the respective photoacoustic curve is the absence of the non-linearities associated with the acoustic Helmholtz resonances in the latter method.[6] These resonances are difficult to eliminate from any microphonic photoacoustic cell[31] and can seriously complicate depth-profiling and thermal characterization of condensed matter specimens. In order to obtain readily interpretable photopyroelectric frequency-response profiles from thin-film PVDF transducers, operation in a frequency range $f >> (2\pi\tau_T)^{-1}$ is recommended, where τ_T is the thermal time constant of the equivalent circuit, given by[32]

$$\tau_T = H/G_T. \tag{12}$$

In Equation (12) H is the thermal capacity of the pyroelectric material and G_T is the thermal conductance to the surroundings. Typically $\tau_T \simeq 0.1-10$ s, for which $f_{\min} >> 1.6$ Hz. In this limit the voltage responsivity $R_v \propto f^{-1}$ a familiar trend shared with other photoacoustic and photothermal detectors.[2] Figure 7 shows the effect of the electrical circuit elements on the frequency response of a PVDF calorimeter.[7] In the current response mode, the time derivative in Equation (11) tends to eliminate the $1/f$ signal dependence, which is present due to the decrease with increasing modulation frequency of the optical energy input into the pyroelectric system per modulation period. For non-ideal amplifier/detection electronics, the electrical circuit of Figure 4 yields a frequency-domain photopyroelectric

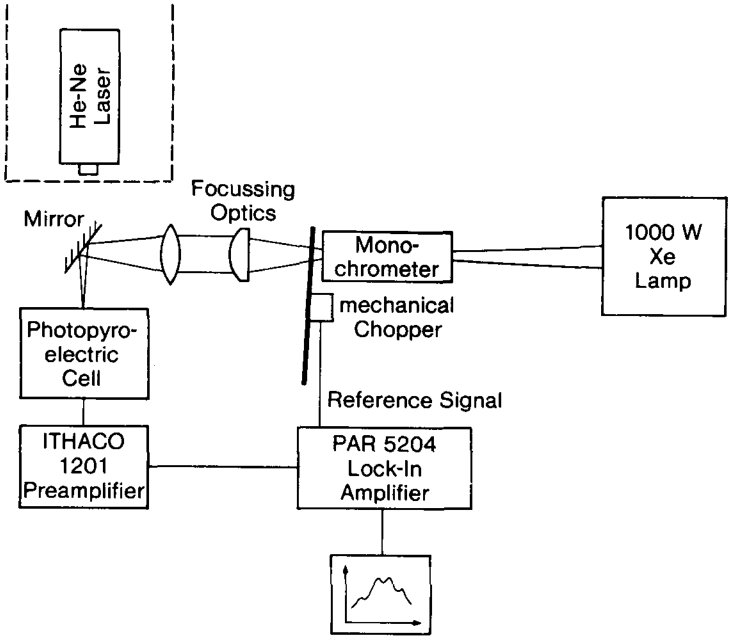

FIGURE 6 Frequency-domain photopyroelectric experimental apparatus. Either a broadband source or a cw laser may be used as shown.[6]

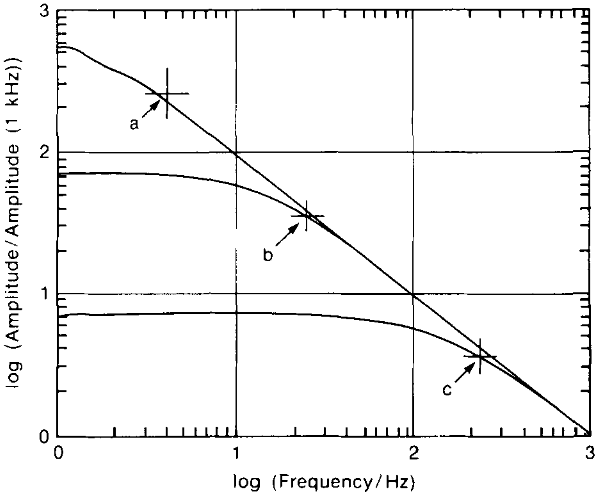

FIGURE 7 Frequency response of a pyroelectric calorimeter with a capacitance $C_p = 600$ pF and a resistance $R_p = 150$ MΩ excited by a light source of constant amplitude, but varying frequency. A lock-in amplifier with 40-pF input capacitance and 100-MΩ input resistance was used for detection. The signal was detected (a) without a load resistor, $R = 60$ MΩ; (b) with a 12.2-MΩ parallel resistor, $R = 10.2$ MΩ; and (c) with a 1.065-MΩ resistor, $R = 1.05$ MΩ. For all three cases the respective corner frequencies and −3 dB points are marked with a (+).[7]

response in the limit of optically opaque pyroelectric transducer as follows[33]

$$V(f) = \frac{2\pi i f p A R \overline{\theta_p(f)}}{1 + i(f/f_E)} \, c^{2\pi i f t} \tag{13}$$

where $f_E = 1/2\pi\tau_E$ and $\overline{\theta_p(f)}$ is the spatial average of the temperature oscillation in the transducer.[15] When the effect of the thermal coupling coefficient between a thin-film pyroelectric and its supporting (backing) material is taken into account, the flat region of the frequency responses shown in Figure 7 turns to a maximum[33,34] across the transition region between thermally thick and thermally thin pyroelectric transducer.[15]

3.3. *Time-Delay (Frequency-Multiplexed) Domain Analysis*

Frequency-multiplexed photopyroelectric excitation and detection is a family of techniques intermediate between time and frequency domains, which has been steadily gaining popularity in recent years. A comprehensive review of general photothermal instrumentation for this group of techniques has appeared elsewhere.[35] Depending on the nature of the pseudo-random photothermal excitation of a pyroelectric transducer, particular members of this family may be discerned. The main common advantages of these methods over conventional time- and frequency-domain techniques include their high-efficiency light-intensity modulation cycle, fast transfer function and impulse-response data acquisition rate, low peak power delivery with the concomitant substantial increase in optical damage threshold of samples, and relative ease of theoretical interpretation of impulse responses (i.e., the system Green's functions themselves, rather than their convolutions). In particular, frequency-sweep modulation (FM linear chirp) excitation has exhibited superior dynamic range in a multiresonant acoustic system (27 dB higher peak response) over its response to an acoustic pulse.[36] No such direct comparison, however, has been reported with photothermal systems.

In applying such techniques to photopyroelectric systems, Coufal[37] used a random number sequence to modulate the intensity of a He–Ne laser beam, so as to excite thin-film samples deposited on a PVDF calorimeter. In this noise modulation scheme, the intensity modulation amplitude is expected to be proportional to the value of a random number generated by a linear congruential sequence at a specific instant. Fast Fourier transformation (FFT) of the correlated input-output data leads to frequency-domain recovery of the system response, namely its transfer function $H(f)$. A similar 28 μm-thick PVDF element was used by Power and Mandelis[38] with a quartz sample as a thermal-wave delay line, in order to compare the instrumental performance under FM chirp and pseudo-random noise excitation, supplied by an HP 3562A dynamic signal analyzer. Fast signal recovery was achieved by FFT methods. Both modulation sequences were found to yield high-quality, band-limited impulse-response information. The pseudo-random noise measurements were much less susceptible to distortions and nonlinearities in the excitation wave train. The FM chirp, however, showed superior coherence and dynamic range. Figure 8 shows a typical experimental set-up for frequency-multiplexed photopyroelectric instrumentation and impulse-response detection.[39] When this instrumentation is used with any of the various excitation waveforms discussed above, it amounts to a spectrometric (i.e., signal-frequency component monitoring) apparatus, which yields information on the relative delay of the system response with respect to the timing of the input excitation. Therefore, the alternate name of Time-Delay Spectrometry (FM-TDS) has been adopted in photothermal applications, as well.

In a recent development, Power introduced amplitude and phase modulation

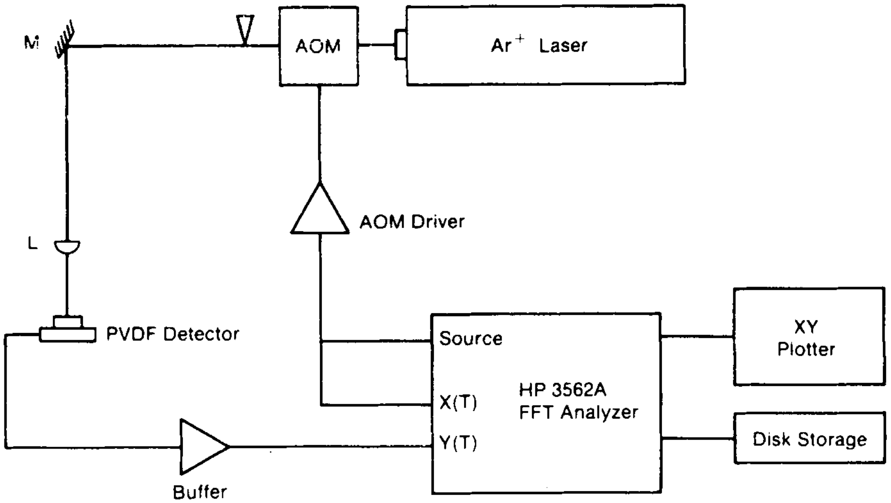

FIGURE 8 FM time-delay photopyroelectric spectrometry apparatus AOM: Acousto-optic modulator; M: Mirror; L: Lens.[39]

(AM-PM) wide-band photopyroelectric spectrometry,[40] a frequency-multiplexed technique akin to FM chirp spectrometry.

Overall, the FM-TDS method has been shown to exhibit much superior SNR advantage over other frequency-multiplexed pseudo-random excitation methods,[39] when applied as a deterministic waveform, since repeated frequency sweeps and response functions may be averaged over time to reduce noise by a factor of $1/\sqrt{N}$. Time-averaged coherence functions of PVDF photopyroelectric signals gave ideal behavior (i.e., unity) from 0–100 kHz, over ten sets of $N = 300$ averages. The equivalent coherence function behavior without averaging (corresponding to nondeterministic pseudo-random excitation) was essentially zero above 10 kHz.

4. SENSORS

A pyroelectric material with optimum thermal and electrical properties has to be selected and the geometry of the element has to be carefully optimized to achieve the best overall performance of the detector. These requirements will depend on the type of excitation (single pulse or periodic) and the mode of application (thermometer or calorimeter). For the following discussion, excitation by one single pulse is assumed at first. Periodic excitation will be discussed subsequently.

For a thermometer it is crucial that its impact on the temperature to be determined be negligible. With a calorimeter a maximum temperature increase for a certain heat input is desirable. In both types of applications the heat capacity of the detector should therefore be small, i.e., the transducer material should have a low density and low specific heat. One of the electrical requirements would be a large pyroelectric coefficient to generate as large a charge as possible for a given temperature rise. To prevent leakage of this charge, low electrical conductivity of the pyroelectric material, or a large sensor resistance R_p, are essential. In addition, a small dielectric constant of the material is desirable to convert the induced charge into as high a voltage as possible. A combination of the most relevant thermal and electrical properties can be represented by a so-called pyroelectric figure of merit.[21] In addition to a large figure of merit, a high Curie temperature, T_c, would be desirable. Operation well below T_c would essentially eliminate the temperature dependence of the pyroelectric coefficient and aging of the sensor material by slow permanent depolarization. Since the pyroelectric coefficient p is proportional to the temperature dependence of the polarization, operation of the sensor at temperatures $T << T_c$ will result, however, in small signal amplitudes.

Inorganic materials such as barium titanate, lithium tantalate, lithium sulfate monohydrate or triglycine sulfate are available as pyroelectric ceramics or single crystals with an excellent figure of merit (up to 15) and a T_c of several hundred °C. These materials are, however, very fragile and hence difficult to handle. Due to cost of the order of several hundred dollars for an element, the use of these materials is limited to special applications such as laser power or energy meters. These materials are bakeable and can be used under UHV conditions without outgassing problems. "Edge-on" electrodes are sometimes employed in these detectors to obtain very high time resolution.

On the other hand, polymer electrets such as β-Polyvinylidene Fluoride[20] (β-

PVDF) are readily available as thin, flexible films with a thickness of several micrometers at cost of \$0.10 per cm^2 and have acceptable thermal, electrical and mechanical properties. β-PVDF has a pyroelectric figure of merit of 9.7 and a T_c of approximately 205°C. In addition, it is compatible with most solvents, media and chemical processes and can be utilized in UHV systems when appropriate precautions are taken. The only drawback of this material is that its use is restricted to stationary temperatures below 200°C. In a pulsed mode, however, transient temperatures up to 900°C can be sustained for several nanoseconds without noticeable degradation of the material.[41] The low cost of the detector material allows disposable detectors, a fact that is of particular interest in routine applications as a thin film monitor. Large area detectors or large numbers of detectors also benefit, of course, from the low cost. In the remainder of this paper the emphasis is therefore placed on β-PVDF as a detector material.

Coated and uncoated poled β-PVDF films are commercially available from Kureha Chemical Industries (KF-Film), Pennwalt Corporation (KYNAR®) and Solvay Technologies (SOLEF®). Representative results on the polarization distribution in foils from these manufacturers have been reported elsewhere. Spin coating or casting of β-PVDF films from a solution,[8,42] or laser sputtering[43] are techniques that allow depositing the detector on a sample rather than depositing the sample on the detector.

Besides these material parameters, the geometry and the dimensions of the element deserve consideration. Being a thermal detector, the coupling area to the sample should be large to facilitate thermal contact. The heat capacity should be small, as mentioned above, and thermal losses from the detector to the surrounding should be kept to a minimum. All of these thermal requirements are best met by a thin pyroelectric film as the detector. In a thermometer a thin pyroelectric film has the additional advantage of a faster response time. For a calorimeter a thin self-supporting film has a smaller lateral heat loss than a thicker material.

In the above design considerations, it was implied that the sample is excited by one single pulse. In that case, heat loss from the sensor to the support ought to be minimized to make the pyroelectric sensor a true calorimeter. For repetitive pulsed or periodic excitation, it becomes, however, imperative to allow sufficient energy loss to the heat sink. It has to be ensured that, averaged over a number of excitation cycles, heat input into the sensor and heat losses are balanced. The temperature in the detector would otherwise increase to the point where the underlying assumption of a temperature independent pyroelectric coefficient is no longer valid, or irreversible damage by overheating of the element occurs. The same argument holds true for the sample being deposited on the calorimeter or attached to the pyroelectric thermometer.

Two thermal diffusion processes are involved in signal generation. Diffusion from the sample into the sensor has been characterized by a transit time τ_t (5). In a similar fashion, diffusion from the sensor element into the surroundings can be described by a heat loss time constant, τ_L, which for one dimensional heat flow would be given by

$$\tau_L = \frac{\ell_p^2}{6\beta_p}, \tag{14}$$

with ℓ_p being the distance between the excited area and the heat sink and β_p the thermal diffusivity of the pyroelectric material. With pulsed excitation, time resolution is normally of paramount interest. In that case the thermal transit time τ_t across the sample should be as short as feasible, i.e., the sample under study should be as thin as possible. Heat loss characterized by the time constant τ_L should be much longer than the thermal transit time τ_t to qualify the detector as a calorimeter. In the remainder of this review applications are discussed, many of them using PVDF thin film sensors in a configuration that is discussed in more detail elsewhere.[7,6]

5. APPLICATIONS

5.1. *Thermal Analysis*

5.1.1. *Surface studies.* Several advances in the spectroscopy of surfaces and adsorbates have been made using pyroelectric detection. Polarization modulation spectroscopy is based on the selective absorption of either *s*- or *p*-polarized light waves, phase-shifted by 180°. The technique has been applied as a real-time compensation scheme by adjusting the relative amplitude of the electric field vector for the two polarizations, in such a way as to obtain a zero substrate signal from an Ag film evaporated *in situ* directly on a pyroelectric ceramic sensor.[44] Then NH_3 molecules were slowly allowed to adsorb on Ag under UHV conditions, giving rise to a photothermal signal due to the selective absorption of the *p*-polarized light of a cw CO_2 laser tuned to 9.30 μm (1075 cm^{-1}) to excite the ν_2 vibrational transition of NH_3. This detection method permits recording photothermal signals induced by an *unstabilized* cw laser with a sensitivity of fractions of a monolayer (e.g., 5×10^{-3} of a monolayer for the NH_3-Ag system, Figure 9). Furthermore, without employing compensation or signal averaging techniques, a sensitivity corresponding to a surface coverage of 2×10^{-3} of a monolayer of SF_6 on silver was achieved under UHV conditions.[45] Under similar conditions, time-dependent phenomena like the adsorption/desorption cycle of SF_6 on silver[46] and the adsorption of NH_3 on silver[47] were readily observed.[47] Coufal[5] carried out surface spectroscopic pyroelectric studies of a Nd_2O_3 sample containing 8×10^{14} molecules isolated in a 10 μm thick poly(methyl methacrylate) matrix, corresponding approximately to a one-monolayer coverage of Nd^{3+} ions, using a PVDF detector. Photothermal spectra were thus obtained under both harmonically modulated and pulsed dye laser excitation in the 400–700 nm region. Figure 10 shows the low-frequency, absorption-like spectrum, demonstrating the strong spectroscopic potential of the photopyroelectric technique for surface species characterization at a sensitivity of hundredths of a monolayer. Pyroelectric *in-situ* detection of the reduction of a film CuO surface oxide layer into metallic Cu by diluted HCl has further demonstrated the ability of the method to monitor interfacial chemistry and measure rate constants.[6]

5.1.2. *Thermal properties.* The capability of photopyroelectric detection to perform thermal-wave depth profiling and selectively monitor conductive transport in photothermally saturated matter[15] places it at an advantage for measuring thermal

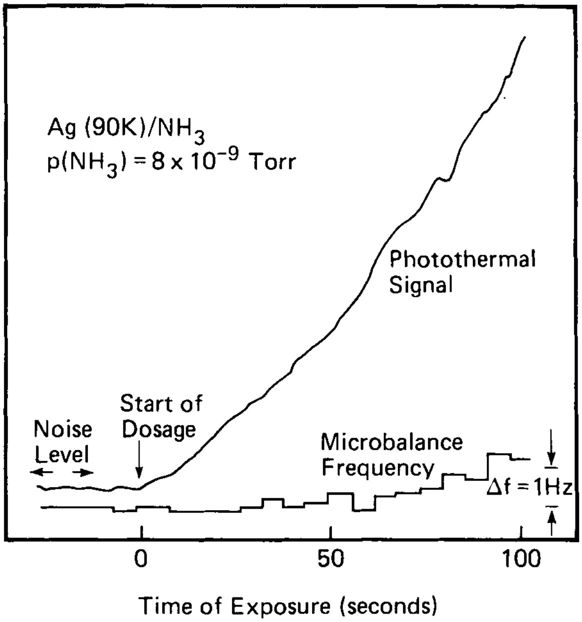

FIGURE 9 Polarization-modulated photopyroelectric signal and microbalance readout as a function of time as ammonia molecules are slowly adsorbed on the silver substrate. The maximum coverage is $\theta = 0.80$. The noise level is indicated on the left hand side for the clean substrate. Shortly before the dosage is started, the noise increases slightly while the dosage valve is opened. The ammonia partial pressure in the system is 8×10^{-9} Torr.[44]

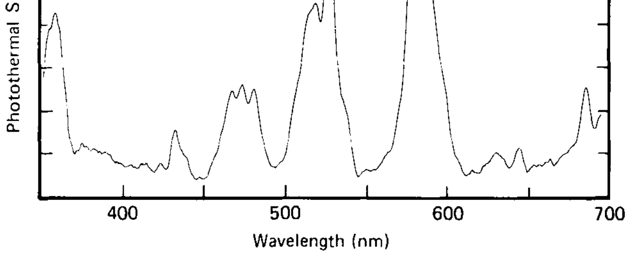

FIGURE 10 Pyroelectric photothermal absorption spectrum of 0.8×10^{15} Nd_2O_3 molecules isolated in a 10 μm thick PMMA matrix recorded in a conventional scanning spectrometer. Modulation frequency: 5 Hz; resolution: 3 nm.[5]

properties, especially thermal diffusivity. Yeack *et al.*[22] used a PZT pyroelectric detector and pulsed CO_2 laser excitation to measure the diffusivity β_s of thin Mylar films, surface-coated with an opaque nichrome film to assure a surface heat source configuration. The fit of a one-dimensional transient heat conduction theoretical expression in Equation (9) to the data was good, especially in the neighborhood of the transient peak, the temporal position of which is sensitive to the value of thermal diffusivity. This yielded an accurate value for β_{Mylar}. More recently Power and Mandelis[39] used FM-TDS to obtain the photopyroelectric impulse response from several materials (fused quartz, stainless steel and aluminum) as detected by a thin PVDF film sensor in back-side contact with the sample. The thin-film response was shown to be more sensitive to thermal conductivity values than that from a thick pyroelectric.[48] Figure 11 shows the excellent fit of the theory to the experimental impulse response from quartz. A comparison between the fit at early times of Figure 11 with that by Yeack *et al.*[22] gives unequivocal evidence of the advantages of using FM-TDS over single-pulse excitation in cases where pulse length and response observation times may overlap, even partially. In order to obtain the photothermal impulse response to a laser pulse from a thin-film resin sample (NOVOLAC™ film), free from artifacts due to the PVDF pyroelectric transducer impulse response itself in the sub-ms time domain, Coufal and Hefferle used a quasi-theoretical/quasi-numerical data fitting procedure.[49] This type of procedure is necessary with thin films, when both detector and sample impulse-response temporal domains heavily overlap. It is quite powerful and simple as it

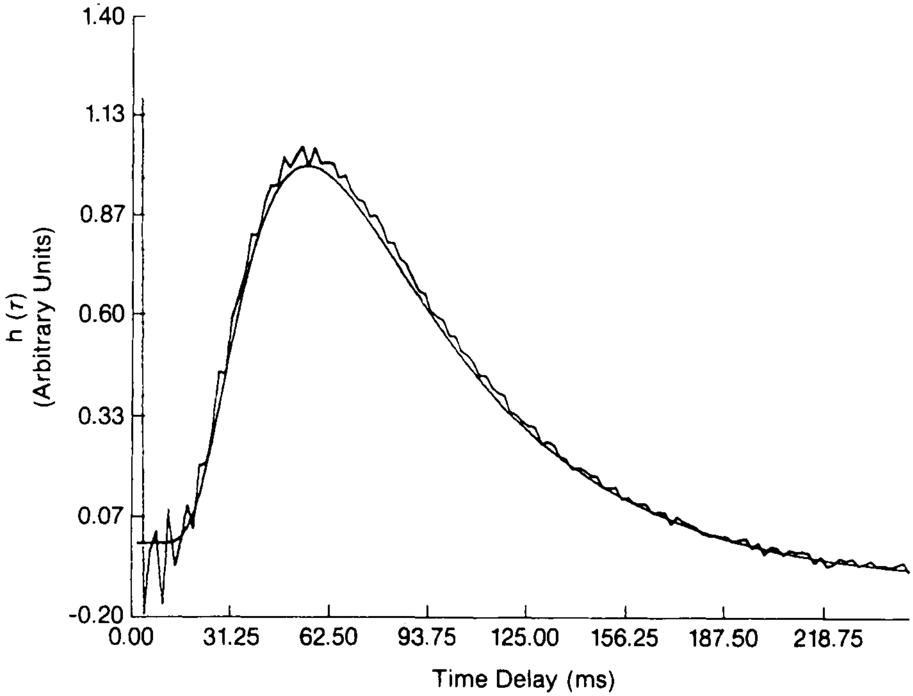

FIGURE 11 Frequency-modulated time-delay-domain (FM-TDS) PVDF photopyroelectric impulse response from a 500-μm quartz sample surface-coated with an opaque thin film. Best fitting parameters to one-dimensional heat conduction model[48]: $\beta_{Quartz} = 4.4 \times 10^{-7}$ m²/s; $k_{Quartz} = 2.2$ W/mK.[39]

accounts for the actual response of experimental pyroelectric circuits without complicating circuit modelling factors, however, it may be altogether avoided with non-thin-film specimens. In such cases appropriate frequency-multiplexed detection techniques and a judicious choice of the exciting frequency bandwidth may be used so that the input signal autocorrelation function and the bare detector input-output cross-correlation function will be delta-function-like in the time scale of the maximum sample response.[35]

A different and very simple method for obtaining accurate values for the thermal diffusivity of materials involves using frequency-domain techniques (either chopped excitation and point-by-point lock-in detection or frequency-sweep excitation and FFT detection) to obtain the laser-induced photopyroelectric transfer function of the sample/detector system. A discontinuity in the amplitude frequency response has been predicted for photoacoustic detection,[18] when the thermal diffusion length in the sample becomes equal to its thickness (i.e., the sample is in the transition region between thermally thick and thermally thin):

$$\mu_s(f) = \left(\frac{\beta_s}{\pi f}\right)^{1/2} \approx L_s. \tag{15}$$

This effect has been demonstrated under photopyroelectric detection as well[6] for a single layer solid; and for a double layer system involving several types of samples (metal, semiconductor and thermal insulator ranging in thickness between 60 μm and 500 μm, and covering several orders of magnitude in thermal diffusivity) supported by a layer of thermally conducting grease[18] on PVDF. Thin-film NOVOLAC™ samples, coated on PVDF, 0.65–2.45 μm thick were successfully analyzed and the diffusivity extracted from the slopes of the transfer functions and from the relative photothermal phase shifts, in a frequency-domain experiment parallel to the pulsed time-domain technique described earlier.[49] Similar photopyroelectric thermal diffusivity measurements in the frequency-domain were recently reported[50] for five polymeric materials (PVDF, PVF, low-density polyethylene, polypropylene. Teflon, as well as a commercial PZT and a tin-substituted PZT). The thicknesses ranged between several micrometers and one millimeter. The thermal diffusivity was estimated by matching the experimental phases to a one-dimensional analytical solution to the heat conduction equation using a minimization algorithm. The resolution and accuracy of the frequency domain photopyroelectric determination of thermal diffusivity of a thin sample are trade-offs between large enough sample thickness and low enough diffusivity to induce a measurable change in slope of the amplitude response or a detectable shift in the phase. A substantial increase in resolution may be effected by modifying the conventional one-dimensional detection geometry[17] as in Figure 12, so that a portion of the lateral dimensions of the sample behaves in a thickness-like manner. Scanning this lateral dimension at fixed modulation frequency has an effect similar to scanning modulation frequencies in the photopyroelectric response, and thermal diffusivity may be readily calculated.

Very recently the photopyroelectric technique was applied to the measurement of thermal parameters of high T_c superconductors. Vitkin *et al.*[51] have demonstrated the sensitivity of the FM-TDS detection method to both thermal diffusivity and thermal conductivity of the $YBa_2Cu_3O_{7-x}$ superconductor. The same authors pre-

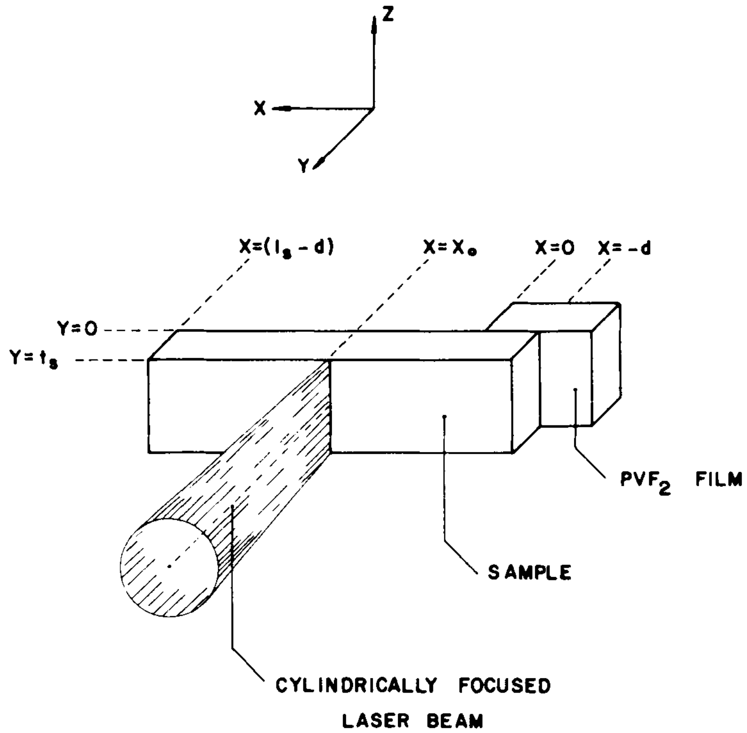

FIGURE 12 Schematic configuration for the photopyroelectric lateral heating method for measuring the thermal diffusivity by scanning the coordinate $x = x_0$.[17]

sented quantitative dependences of those parameters on temperature,[52] using a single crystalline YBCO specimen and relating the impulse-response peak and long-time tail to the diffusivity $\beta_{\mathrm{YBCO}}(T)$ and conductivity $k_{\mathrm{YBCO}}(T)$, respectively, as described earlier (see Figure 11 and relevant discussion in the text). A qualitative functional dependence of the specific heat on temperature was further obtained as a derivative measurement[52] based on the relation:

$$C_{\mathrm{YBCO}}(T) = \frac{k_{\mathrm{YBCO}}(T)}{\rho\beta_{\mathrm{YBCO}}(T)} \tag{16}$$

where ρ is the superconductor density, assumed temperature independent. Similar measurements on ceramic YBCO were reported by Marinelli *et al.*[33] in the frequency domain using a thick $LiTaO_3$ pyroelectric crystal and extensions/special cases of the photopyroelectric theory[15] pertinent to their geometry. A combination of transfer function amplitude and phase data from a calibrated sensor yielded the low-T behavior of thermal diffusivity and effusivity as primary measurements in the range 80–118K. The dependence of $\beta_{\mathrm{YBCO}}(T)$ on $k_{\mathrm{YBCO}}(T)$ and on $C_{\mathrm{YBCO}}(T)$, via Equation (16), and of the effusivity e_{YBCO},

$$e_{\mathrm{YBCO}}(T) = [\rho C_{\mathrm{YBCO}}(T) k_{\mathrm{YBCO}}(T)]^{1/2} \tag{17}$$

further yielded thermal conductivity and specific heat dependences. The potential of photopyroelectric detection in thermodynamic studies of high T_c superconductors appears to be superior to other photothermal techniques, due to its ability to yield multiple parameter measurements simultaneously in a simple, self-consistent and experimentally straightforward fashion. Similar relative advantages have emerged in spectroscopic applications (see below).

5.1.3. *Depth profiling and imaging.* The depth profiling capability of general photothermal detection schemes is well documented[2] and has been mentioned earlier on in this section in relation to the probing of pyroelectric materials themselves. Pulsed laser excitation of thin β-PVDF electrets has been used[7] to determine the depth profile of charge or electric field distributions as results of poling. Frequency-domain photothermal determination of polarization inhomogeneity depth profiles has been modelled and fitted to experimental PVF and PVF_2 transfer functions by Peterson *et al.*[26] Other photothermal variants include the laser-intensity modulation method (LIMM)[53–55] and the photoacoustic laser-induced pressure pulse method (LIPP).[56–59] The amplitude response curve versus square root of modulation frequency of the photopyroelectric signal has been shown[15,18] to involve a change in slope at frequencies where the thickness of a material layer becomes equal to the thermal diffusion length, Equation (15). This property can be utilized as a simple and accurate depth profiling method to identify multi-layer geometries, if thermal diffusivities are known, or otherwise for non-destructive identification of discontinuous sub-surface boundaries.

Conventional pyroelectric detection of thermal waves used in a scanned, spatially-integrated detection mode has been reported for some time.[60,61] A scanning photopyroelectric application using a silicon wafer with a man-made defect in contact with PVDF has demonstrated the ability of the technique to perform photothermal microscopy of samples with sub-surface defects.[62] Recently, spatially resolved photothermal scanning imaging using the photopyroelectric effect was reported.[63] Thermal wave information was obtained with a PVDF film sensor unelectroded on one side facing a thin metal probe tip. A modulated photothermal source on the surface of the sample induced an oscillating temperature field in the pyroelectric material, which produced a displacement current proportional to the temperature change. The effects of this current on the charge density of the unelectroded surface were monitored as a synchronous change in the space capacitance between the PVDF film and the probe tip, Figure 13. The oscillating capacitive voltage was thus used to provide a means for measuring the *local* values of laser-induced diffractive[64] and/or interferometric[65] thermal wave fields in metallic samples. Quantitative comparisons with a diffraction-integral approach of the thermal wave field at the back surface of a sample[66] have been presented[65] and the role of the tip size as the most important factor limiting spatial resolution of the microscopy has been studied.[65] A recent development of spatially resolved, laser-beam and probe-tip scanned photopyroelectric imaging has produced spatial frequency-multiplexed interferograms, the reconstruction of which is in progress[67] and is expected to lead to photopyroelectric Thermal Wave Tomography.[68]

5.1.4. *Phase transitions.* In addition to providing information concerning material thermal parameters (e.g., diffusivity, effusivity, conductivity) pyroelectric thermal wave detection was shown to be sensitive to first and second order thermodynamic phase transitions in bulk solids.[69] Unlike conventional photoacoustic

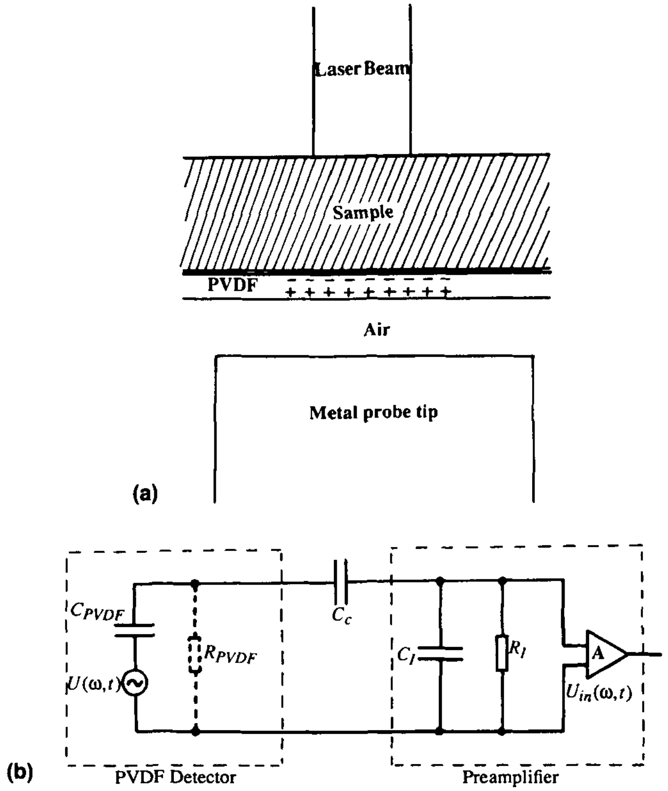

FIGURE 13 (a) Schematic diagram of the capacitively-coupled pyroelectric geometry used for scanning microscopy of spatially resolved thermal waves in condensed phase materials; (b) Electrical equivalent circuit diagram for contactless photopyroelectric detection: $U(\omega, t)$ is the pyroelectric voltage generated across the PVDF film. $U_{in}(\omega, t)$ is the input voltage across the amplifier A. Besides the capacitive (C_{PVDF}, C_l) and resistive (R_{PVDF}, R_l) elements in the detector and preamplifier, respectively, the space capacitance at the PVDF unelectroded surface/probe tip interface is shown as C_c.[63]

detection of phase transitions,[70] the back-surface pyroelectric detection provides a signal proportional to the thermodynamic quantity of interest, i.e., the specific heat,[69] rather than the product of specific heat *and* thermal conductivity.[70] These experiments on model systems established the frequency-domain method and the associated theory for the study of phase transitions. More recently, the time-domain method was applied to real-time studies of laser annealing.[71] With first order phase transitions the direct time-domain observation seems to be preferable. For second order transitions, however, frequency-domain detection has shown unique potential, with distinct advantages in experimental simplicity and theoretical interpretability over conventional photoacoustic methods. Very recently, the emerging capabilities of photopyroelectric detection to monitor superconducting phase transitions have been demonstrated.[33,51,52] The potential to obtain more than one thermodynamic parameters, and their temperature dependences, simultaneously from the photopyroelectric signal (see Equations (16) and (17)), coupled with relative experimental simplicity (including cryogenics), compares very favorably with other photoacoustic[72] and photothermal[73] detection schemes.

5.2. *Spectroscopy*

5.2.1. *Reflectivity studies.* When a sample is directly deposited onto a pyroelectric element, the observed signal is proportional to the absorbed energy only, i.e., to I_0 $[1\text{-}R(\lambda)]$, where I_0 is the incident intensity and $R(\lambda)$ the reflectivity of the sample. Burns *et al.*[28] first used a pyroelectric $Pb_5Ge_3O_{11}$ sensor to monitor the reflectivity spectrum of a gold film; they also drew attention to the potential use of the technique to measure the optical absorption of thin layers of materials coated on a reflecting electrode of a pyroelectric sensor. Subsequently, the change in the reflectivity of an oxidized Cu surface during reduction was used to monitor the course of the chemical reaction photopyroelectrically (see Section 5.1. above).[6] Absorbing samples supported by reflecting pyroelectric sensors can exhibit spectral artifacts, especially in semi-transparent regions where both sample and reflecting electrode wavelength-dependence contribute to the photopyroelectric signal. Chirtoc and coworkers demonstrated these artifacts in the infrared spectrum of water[74] and developed a detailed theoretical analysis of the various resulting distortions and peak inversions of condensed phase spectra obtained with periodic excitation.[75] At this time it is clear that reflection-induced spectral artifacts can be satisfactorily eliminated[76] by coating or spray-painting the pyroelectric sensor electrode black, which obviates the need for very complicated theoretical requirements[75] in order to obtain quantitative absorption spectra. Taking advantage of the electrode reflections may, on the other hand, yield pyroelectric spectra of adsorbates on reflecting metal surfaces.[16] In a modern recreation of Wiener's classical experiment on the phase change of a light wave upon reflection from an optically denser medium,[77] the standing light wave in front of a metal reflecting mirror (the Ag electrode of a PVDF detector) was mapped.[78] In that experiment, the quenching of an excited state was studied as a function of distance from the mirror with a spatial resolution of several nm.

5.2.2. *Absorption coefficient spectra.* Photopyroelectric spectroscopy has been very successful in monitoring absorption spectra of a variety of condensed phase materials, thus providing a simple, inexpensive alternative to conventional photoacoustic spectroscopy.[2] Section 5.1 has already dealt with applications to the spectroscopy of surface adsorbates. With thin layers of finite thickness compared to the thermal diffusion length, deposited directly on the pyroelectric sensor, absorption spectra may be obtained qualitatively.[5,6] Care must be taken to operate at a low modulation frequency where the sample is entirely thermally thin; then the photopyroelectric signal, when properly source-compensated (normalized), replicates the optical *absorption* spectrum, subject to the requirement for spectrally flat nonradiative quantum yield.[15] Figure 10 is an example of such a spectrum. At high modulation frequencies, such that the sample is entirely thermally thick, the normalized photopyroelectric signal replicates the optical *transmission* spectrum, regardless of the spectral variation of the nonradiative quantum yield.[15] This is demonstrated in Figure 14 for the sample of Figure 10.[16] Any intermediate modulation frequency yields spectra grossly distorted due to competing optical and thermal-wave contributions to the pyroelectric signal.[6] For very thin films, transmission or absorption pyroelectric spectra may be conveniently obtained using pulsed excitation with a continuously (or line) tunable laser and time-gating de-

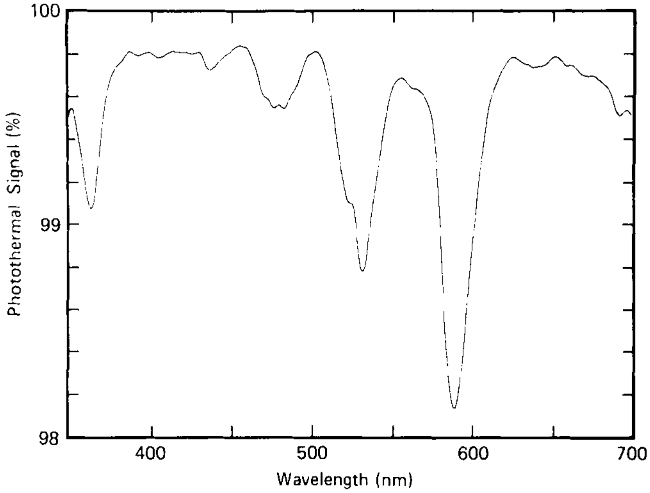

FIGURE 14 Pyroelectric photothermal transmission spectrum of the sample in Figure 10, detected with the same detector at 88 Hz. PMMA matrix thickness: 100 μm.[16]

tection methods.[5] An alternative frequency-domain detection scheme of direct photopyroelectric phase discrimination has been proposed.[79] With this method, a *qualitative* measurement of the optical absorption spectrum $\alpha(\lambda)$ can be obtained upon considering only the out-of-phase (quadrature) lock-in signal component at a fixed modulation frequency, by virtue of the fact that all background contributions affect the in-phase component only.[16] Spectra of a thin Nd_2O_3 powder layer were thus simply recorded.

Pyroelectric sensors have further been utilized to study the optical absorption of opaque solids, such as graphite plates,[80] anodized Al plates,[80] powders of rare earth oxides,[6,79] heavily absorbing liquids[74]; and weakly absorbing materials, such as thin solid films,[81] or liquids.[82] Recently, an area of growing importance is photothermal diagnostics of semiconductors.[4] Tanaka *et al.*[83,84] used 7 μm thick PVDF films coated with transparent CuI electrodes of *ca.* 200 Å thickness to record spectra of amorphous As_2S_3 and Se thin films, Figure 15. Thus, the capability of the photopyroelectric method to obtain $\alpha(\lambda)$ spectra free from acoustic noise, of quality similar to PAS and sensitivity of $\alpha l_s \gtrsim 10^{-2}$ was shown. An additional advantage over PAS was pointed out to be the simple requirement for conventional optical cryostats for low-temperature spectroscopy, Figure 15b, unlike the much more complicated cryogenic systems associated with microphonic photoacoustic detection.[85] Mandelis *et al.*[86] established the similarity in quality of photopyroelectric spectra from amorphous thin-film semiconductors to those obtained via photothermal beam deflection spectroscopy. Furthermore, photopyroelectric spectroscopy was found to be sensitive to mechanically introduced defects in semiconductors near the bandgap region,[87] due to an enhancement in nonradiative defect densities and de-excitation probabilities.

5.2.3. *Nonradiative quantum yields and spectra.* Since the heat released in a sample following optical excitation is the operating signal source in every photothermal system, all such probing techniques are dependent on the nonradiative

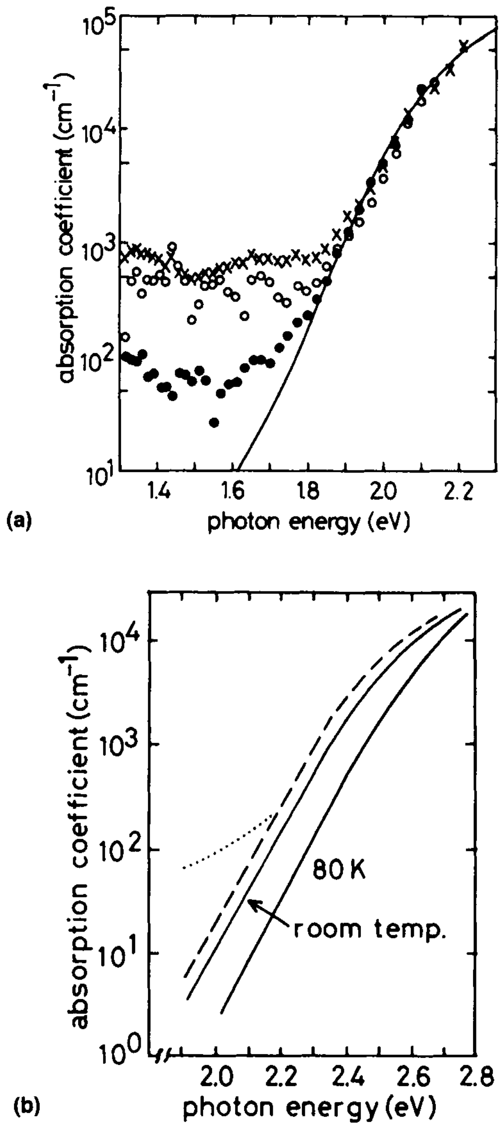

FIGURE 15 (a) The optical absorption edge of amorphous Se evaluated with the photopyroclectric method and from a photoacoustic measurement (solid line). The photopyroelectric data are given for film thicknesses of 1.43 μm (●-●-●); 0.96 μm (o-o-o); and 0.74 μm (×-×-×). (b) The optical absorption edges of an annealed As_2S_3 film at room temperature and at 80 K (solid lines). The characteristics at room temperature after optical annealing (dashed line) and during annealing (dotted line) are also shown.[84]

quantum yield $\eta(\lambda)$ of the monitored optical-to-thermal energy conversion process. Pyroelectric detection is ideally suited for the determination of $\eta(\lambda)$ among photothermal methods, by virtue of its back-surface character. To demonstrate how this can be achieved, consider the trilayered sample shown in Figure 16, with a weakly absorbing layer 1, of absorption coefficient $\alpha_1(\lambda)$ and nonradiative quantum

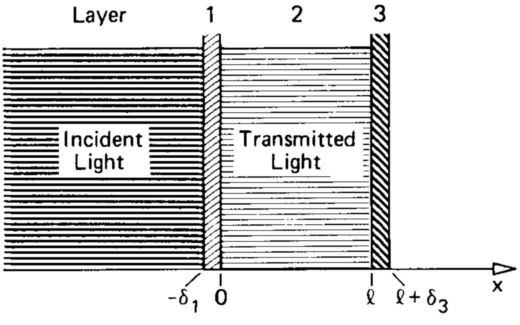

FIGURE 16 A composite trilayered sample geometry for the determination of nonradiative quantum yields.[16]

efficiency $\eta_1(\lambda)$, separated from another absorbing layer 3 by a transparent spacer layer 2. The photopyroelectric signal at the back interface 1 and at modulation frequency f is given by[16,86]:

$$S(\lambda, f) = C(f)I_0(\lambda)\{\eta_1(\lambda)A_1(\lambda)\exp\,[-(1 + i)l/\mu_2(f)] + A_3(\lambda)\eta_3(\lambda)T_1(\lambda)\} \quad (18)$$

where $C(f)$ is an assortment of instrumental and geometric parameters of the sample-PVDF detector system; $A_i(\lambda)$, $\eta_i(\lambda)$ and $T_i(\lambda)$ are the absorbance, nonradiative quantum yield, and transmittance of the i-th layer, respectively; and $\mu_2(f)$ is the thermal diffusion length in the spacer layer. From the structure of Equation (18) it can be seen that at high f (thermally thick limit) only the in-phase term is present and the spectrum can be manipulated to give $\alpha_1(\lambda)$ through the $T_1(\lambda)$ term. Another low-f spectrum (thermally thin limit) may then be recorded, with the $\alpha_1(\lambda)$ data (and the known spacer thermal diffusivity) substituted from the high-f spectrum, to yield the $\eta_1(\lambda)$ spectrum simply and self-consistently. Figure 17 shows one such example from a thin a-Si:H film.[86] Quantum yields at single wavelengths have also been determined for thin-film samples.[5,16,78] The dramatic spectral variations in $\eta_{si}(\lambda)$ observed in Figure 17b indicate that due attention must be paid to this channel and that the usual simplifying assumptions about its value[84] or its constancy[79] must only be used cautiously and with appropriate justifications.

Metal surfaces with well-defined periodicity can be produced on PVDF sensors using a holographic technique,[88] allowing to couple light into the plasmon surface polariton and to conveniently study the plasmon dispersion, as well as the influence of dielectric adsorbates and thin films on the resonance shift. With a diffraction grating on the sample surface, instead of the conventional prism coupler used with photoacoustic attenuated total reflection,[89] the photothermal detection of plasmons was found to be enhanced.[90]

Recently, Fourier transform infrared photopyroelectric spectroscopy (FTIR-PPES) was introduced[91] as a new technique capable of experimentally convenient qualitative analysis and theoretically relatively simple quantitative calculation. It was found that an experimentally derived numerical correction is required for spectra obtained in the thermally thick limit. No such correction was found necessary for thermally thin spectra. A comprehensive theoretical framework for FTIR-PPES was also developed, based on principles outlined earlier.[15] The technique appears

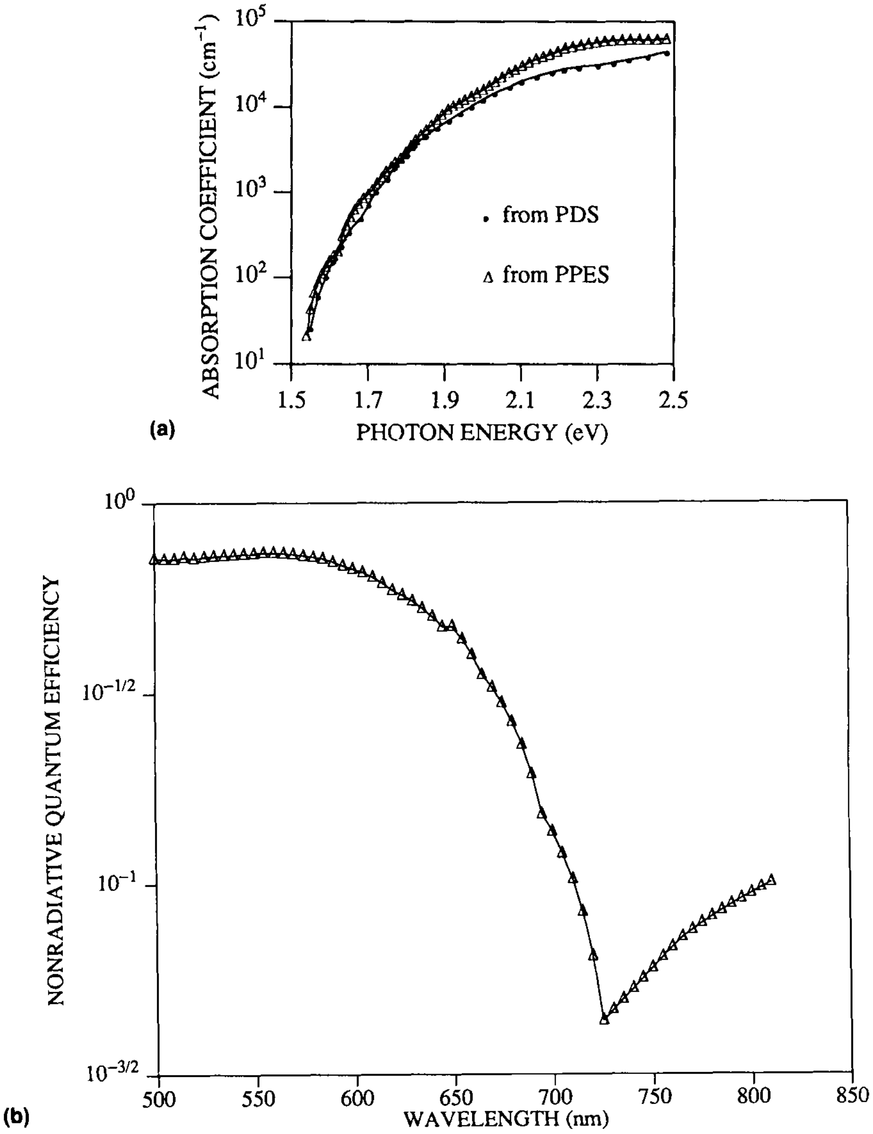

FIGURE 17 (a) Optical absorption coefficient for a-Si:H thin film using photopyroelectric (PPES) and photothermal deflection (PDS) spectroscopies; (b) Nonradiative quantum efficiency specctrum of the same sample.[86]

to be most promising in the study of thin layers[91] and powders[92] deposited directly on PVDF, especially when used to monitor various *in-situ* interactions with external agents (chemical, optical, etc.).

5.3. *Other Applications*

A recent development is a thin-film photopyroelectric gas sensor, a new type of solid-state device for the detection of minute concentrations of hydrogen gas under

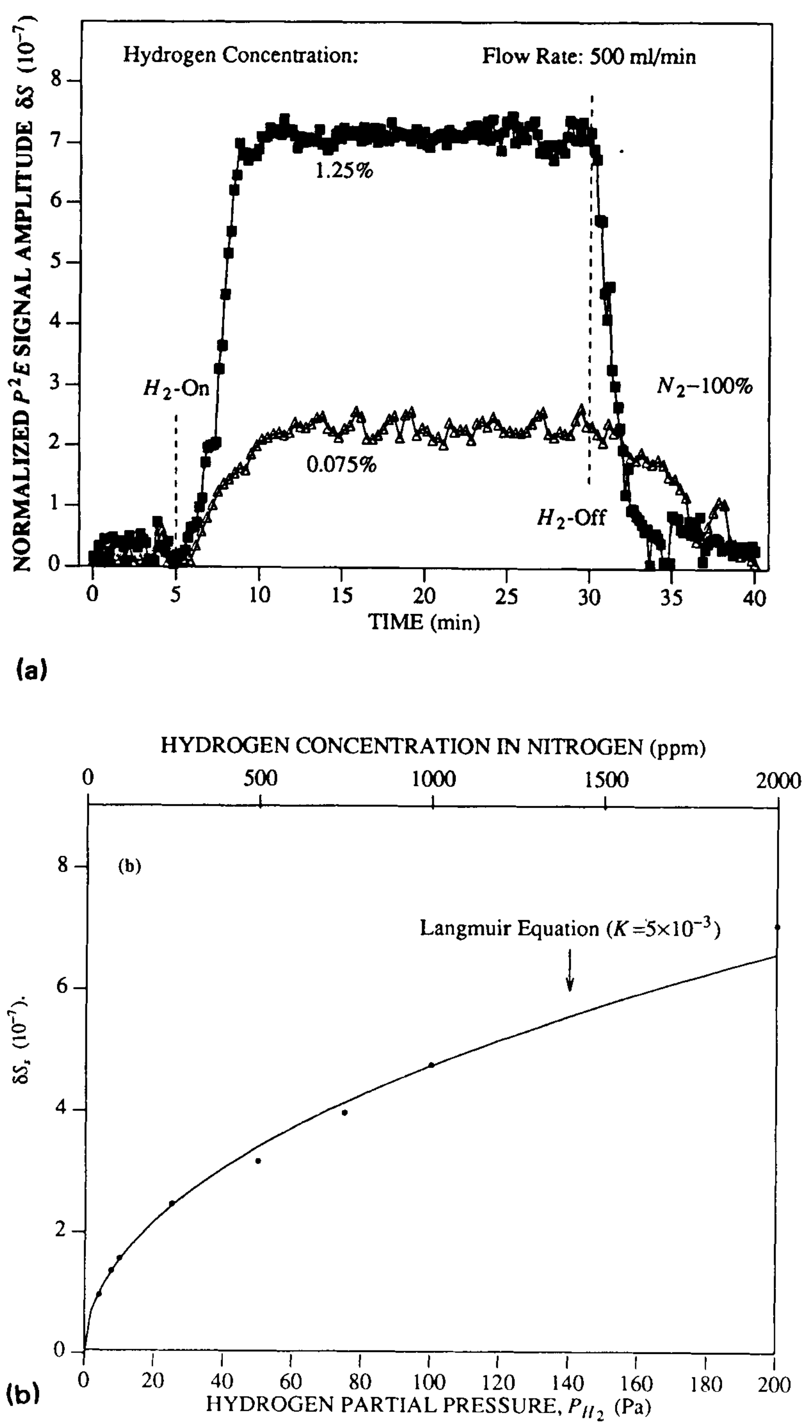

FIGURE 18 (a) Photopyroelectric response as a function of time, for two low H_2 concentrations. Pd thickness = 285 Å; flow rates: 500 ml/min; T = 20°C. (b) Variation of output saturation signal δS_s as a function of partial hydrogen pressure (or concentration). Pd thickness = 130 Å. The solid curve is the fitted Langmuir isotherm.[93]

environmental, flow-through conditions.[93] The sensor was made of thin, commercially available PVDF film, sputter-coated with Pd. An infrared beam from a semiconductor laser diode was coupled to an optical fiber and irradiated the PVDF, thus generating a carrier wave ac photopyroelectric voltage. Sensitivity to exposures in a hydrogen partial pressure has been demonstrated down to concentrations as small as 40 ppm, in a flowing $H_2 + N_2$ mixture. Figure 18 shows typical sensor response curves and signal compliance with a Langmuir isotherm, in agreement with the dissociation reaction

$$H_2 \rightleftarrows 2H_a \tag{19}$$

on the Pd surface.

A review of pyroelectric detection of photothermal wave processes would be incomplete without mentioning work in other spectral ranges, such as the detection of magnetic resonance phenomena[94] or x-ray spectroscopy with synchrotron radiation for excitation.[81]

When replacing electromagnetic radiation by particles the pyroelectric sensor is no longer used as a photothermal detector in a rigorous sense. The potential of the pyroelectric calorimeter for other radiation induced thermal phenomena such as the detection of ultraheavy nuclei[95] is tremendous. Experiments with excited fragments in a molecular beam[96] or the characterization of a free jet expansion highlight the versatility of these detectors. By now a special sensor has been developed for these molecular beam applications.[97] Recently the energy transfer from ablated fragments to a pyroelectric calorimeter was utilized to study the products of ultraviolet laser ablation from polymers.[98] Studies of energy transfer from energetic ions to thin films with pyroelectric calorimeters shed light into issues such as ion etching or the interaction of the plasma with the wall in a fusion reactor.[99]

6. CONCLUSION

Pyroelectric sensors have been demonstrated to be extremely powerful detectors for thermal wave phenomena. With pulsed excitation thermal transients can be studied directly in the time domain with utmost sensitivity and time resolution. Using conventional single frequency or noise amplitude modulation, frequency domain experiments can be performed over an extremely wide dynamic range and bandwidth. The unique potential of pyroelectric detection for thermal transients and spectroscopy of surfaces, thin films and bulk samples has been exemplified and new imaging applications for non-destructive evaluation of materials have been reviewed. The importance of the ferroelectric characteristics of the sensor material has been emphasized whenever appropriate and directions for improvement pointed out.

ACKNOWLEDGEMENTS

We would like to thank our colleagues in this rapidly expanding field for numerous enlightening discussions, for their helpful comments and for sharing information prior to publication. It is a privilege to thank our collaborators for their numerous contributions. They were instrumental in advancing this field!

One of us (A.M.) wishes to acknowledge the support of the Natural Sciences and Engineering Research Council of Canada (NSERC) and that of the Ontario Laser and Lightwave Research Center (OLLRC) and the Ministry of Energy, Mines and Resources (EM&R), regarding various aspects of research presented in this review article.

REFERENCES

1. Y. H. Pao, *Optoacoustic Spectroscopy and Detection* (Academic, New York, 1977).
2. A. Rosencwaig, *Photoacoustics and Photoacoustic Spectroscopy*, Chemical Analysis, Vol. 57 (Wiley, New York, 1980).
3. V. P. Zharov and V. S. Letokhov, *Laser Optoacoustic Spectroscopy*, Springer Ser., Opt. Sci., Vol. 37 (Springer, Berlin, Heidelberg, 1986).
4. A. Mandelis (ed.), *Photoacoustic and Thermal Wave Phenomena in Semiconductors* (Elsevier, Amsterdam, 1987).
5. H. Coufal, *Appl. Phys. Lett.*, **44,** 59 (1984).
6. A. Mandelis, *Chem. Phys. Lett.*, **108,** 388 (1984).
7. H. Coufal, R. Grygier, D. Horne and J. Fromm, *J. Vac. Sci. Technol.*, **A5,** 2875 (1987).
8. H. Coufal and R. Grygier, *J. Opt. Soc. Am.*, **B6,** 2013 (1989).
9. H. Coufal, *IEEE Trans.*, **EI-21,** 495 (1986).
10. H. Coufal, *IEEE Trans.*, **UFFC-33,** 507 (1986).
11. S. B. Lang, *Sourcebook of Pyroelectricity*, (Gordon and Breach, London, 1974).
12. T. J. Negran, *Ferroelectrics*, **34,** 31 (1981).
13. H. S. Carslaw and J. C. Jaeger, *Conduction of Heat in Solids*, (Oxford University Press, Oxford, 1959).
14. J. Fromm and H. Coufal, in *Photoacoustic and Photothermal Phenomena*, (P. Hess and J. Pelzl, eds., Springer Ser. Opt. Sci., Vol. 58, Heidelberg, p. 164 (1988).
15. A. Mandelis and M. Zver, *J. Appl. Phys.*, **57,** 4421 (1985).
16. H. Coufal, *Appl. Phys. Lett.*, **45,** 516 (1984).
17. C. C. Ghizoni and L. C. M. Miranda, *Phys. Rev.*, **B32,** 8392 (1985).
18. P. K. John, L. C. M. Miranda and A. Rastogi, *Phys. Rev.*, **B34,** 4342 (1986).
19. W. R. Belvin and J. Geist, *Appl. Opt.*, **13,** 1171 (1973).
20. For information on PVDF see *Ferroelectrics* **32,** (1981); data concerning KYNAR® can be found in *Pennwalt KYNAR® Piezo Film Technical Manual* (Pennwalt, King of Prussia, 1983); for other ferroelectrics, *Proceedings of the 6th International Symposium on Electrets*, Oxford 1988, D. K. Das-Gupta and A. W. Patullo, Eds., IEEE Service Center Piscataway, New Jersey.
21. R. L. Byer and C. B. Roundy, *Ferroelectrics*, **3**, 333 (1972).
22. C. E. Yeack, R. L. Melcher and S. S. Jha, *J. Appl. Phys.*, **53,** 3947 (1982).
23. R. W. Whatmore, *Rep. Progr. Phys.*, **49,** 1335 (1986).
24. H. Coufal, in *Photoacoustic, Photothermal and Photochemical Processes at Surfaces and in Thin Films*, P. Hess, Ed. (Springer-Verlag, "Topics in Current Physics," Vol. **47,** Heidelberg 1989) Chap. 5.
25. R. J. Phelan, Jr., R. J. Mahler and A. R. Cook, *Appl. Phys. Lett.*, **19,** 337 (1971).
26. R. L. Peterson, G. W. Day, P. M. Gruzensky and R. J. Phelan, Jr., *J. Appl. Phys.*, **45,** 3296 (1974).
27. R. Gerhardt-Multhaupt, *Ferroelectrics*, **75,** 385 (1987).
28. B. Burns, F. H. Dacol and R. L. Melcher, *J. Appl. Phys.*, **54,** 4228 (1983).
29. G. W. Day, C. A. Hamilton, P. M. Gruzensky and R. J. Phelan, *Ferroelectrics*, **10,** 99 (1976).
30. S. B Peralta, K. Ghandi and A. Mandelis, *Rev. Sci. Instrum.*, **61,** 1038 (1990).
31. N. C. Fernelius, *Appl. Opt.*, **18,** 1784 (1979).
32. E. H. Putley, in *Semiconductors and Semimetals*, R. K. Willardson and A. C. Beer, Eds., (Academic, New York, 1970) Chap. 6.
33. M. Marinelli, F Murtas, M. G. Mecozzi, U. Zammit, R. Pizzoferrato, F. Scudieri, S. Martelucci and M. Marinelli, *Appl. Phys.*, A **51,** 387 (1990).
34. C. Christofides and A. Mandelis, unpublished.
35. A. Mandelis, *IEEE Trans.*, **UFFC-33,** 596 (1986).
36. J. Trampe Broch, *Brüel & Kjaer Tech. Rev.*, **4**, 3 (1975).
37. H. Coufal, *J. Photoacoustic.*, **1**, 413 (1984).
38. J. F. Power and A. Mandelis, *Rev. Sci. Instrum.*, **58,** 2033 (1987).
39. J. F. Power and A. Mandelis, *Rev. Sci. Instrum.*, **58,** 2024 (1987).
40. J. F. Power, *Rev. Sci. Instrum.*, **61,** 90 (1990); and *Rev. Sci. Instrum.*, **61,** 101 (1990).
41. H. Coufal and W. Lee, *Appl. Phys. B.*, **44,** 141 (1987).

42. G. Sessler, *J. Acoust. Soc. Am.*, **70,** 1596 (1981).
43. M. Sirajuddin and J. Reddy, *Thin Solid Films*, **124,** 149 (1984).
44. H. Coufal, F. Träger, T. J. Chuang and A. C. Tam, *Surf. Sci. Lett.*, **145,** L504 (1984).
45. H. Coufal, T. J. Chuang and F. Träger, *IBM Res. Report*, **RJ 4344,** (1984).
46. F. Träger, H. Coufal and T. J. Chuang, *Phys. Rev. Lett.*, **49,** 1720 (1982).
47. T. J. Chuang, H. Coufal and F. Träger, *J. Vac. Sci. Technol.*, **A1,** 1236 (1983).
48. J. F. Power and A. Mandelis, *Rev. Sci. Instrum.*, **58,** 2018 (1987).
49. H. Coufal and P. Hefferle, *Appl. Phys.*, **A38,** 213 (1985).
50. S. B. Lang, *Ferroelectrics*, **93,** 87 (1987).
51. I. A. Vitkin, S. B. Peralta, A. Mandelis, W. Sadowski and F. Walker, *Meas. Sci. Technol.*, **1,** 184 (1990).
52. S. B. Peralta, I. A. Vitkin, K. Ghandi, A. Mandelis, W. Sadowski and E. Walker, in *Photoacoustic and Photothermal Phenomena II*, J. C. Murphy, J. W. Maclachlan Spicer, L. C. Aamodt and B. S. H. Royce, eds., Springer Ser. Opt. Sci., Vol. 62, Heidelberg, p. 211 (1990).
53. S. B. Lang and D. K. Das-Gupta, *Ferroelectrics*, **39,** 1249 (1981).
54. S. B. Lang and D. K. Das-Gupta, *Ferroelectrics*, **55,** 151 (1984).
55. S. B. Lang and D. K. Das-Gupta, *Ferroelectrics*, **60,** 23 (1984).
56. R. Gerhard-Multhaupt, G. M. Sessler, J. E. West, K. Holdik, M. Haardt and W. Eisenmenger, *J. Appl. Phys.*, **55,** 2769 (1984).
57. G. M. Sessler, J. E. West and R. Gerhard, *Phys. Rev. Lett.*, **48,** 563 (1982).
58. R. Gerhard-Multhaupt, *Phys. Rev.*, **B27,** 2494 (1983).
59. G. M. Sessler, R. Gerhard-Multhaupt, J. E. West and H. von Seggern, *J. Appl. Phys.*, **58,** 119 (1985).
60. M. Luukkala, in *Scanned Image Microscopy*, E. A. Ash, ed. (Academic, London, 1980), p. 273.
61. C. R. Petts and H. K. Wikramasinghe, *Proc. IEEE Ultrason. Symp.*, 1981, p. 832.
62. I. F. Faria, Jr., C. C. Ghizoni and L. C. M. Miranda, *Appl. Phys. Lett.*, **47,** 1154 (1985).
63. M. Mieszkowski, K. F. Leung and A. Mandelis, *Rev. Sci. Instrum.*, **60,** 306 (1989).
64. M. Mieszkowski and A. Mandelis, *J.O.S.A.*, **A7,** 552 (1990).
65. A. Mandelis and K. F. Leung, *J.O.S.A.*, A **8,** 186 (1991).
66. A. Mandelis, *J.O.S.A.*, **A6,** 298 (1989).
67. M. Munidasa and A. Mandelis, unpublished.
68. A. Mandelis and A. Mieszkowski, U.S. Patent Number: 4,950,897; Date: August 21, 1990.
69. A. Mandelis, F. Care, K. K. Chan and L. C. M. Miranda, *Appl. Phys.*, **A38,** 117 (1985).
70. M. A. A. Sigueira, C. C. Ghizoni, J. I. Vargas, E. A. Menezes, H. Vargas and L. C. M. Miranda, *J. Appl. Phys.*, **51,** 1403 (1980).
71. H. Coufal and W. Lee, *Appl. Phys.*, **B44,** 141 (1987).
72. L. Gomes, M. M. F. Vieira, S. L. Baldochi, N. B. Lima, M. A. Novak, N. D. Vieira, Jr., S. P. Morato, A. J. P. Braga, C. L. Cesar, A. F. S. Penna and J. Mendes Filho, *J. Appl. Phys.*, **63,** 5044 (1988).
73. J. Fanton, G. S. Kino and B. T. Khuri-Yakub, *IEEE Ultrason. Symp.*, 1093 (1988).
74. M. Chirtoc, D. Dadârlat, I. Chirtoc and D. D. Bicanic, *Spectrosc. Lett.*, **21,** 413 (1988).
75. M. Chirtoc and G. Mihailescu, *Phys. Rev.*, **B40,** 9606 (1989-I).
76. C. Christofides, A. Mandelis, K. Ghandi and R. E. Wagner, *Rev. Sci. Instrum.*, **61,** 2360 (1990).
77. A. Wiener, *Wied. Ann.*, **40,** 203 (1890).
78. W. Knoll and J. H. Coufal, *Appl. Phys. Lett.*, **51,** 892 (1987).
79. Y. Dupin, Z. Angru and W. Zhaoyong, *J. Phys. D.*, **21,** 641 (1988).
80. D. Dadârlat, M. Chirtoc, R. M. Cândea and I. Bratu, *Infrared Phys.*, **24,** 469 (1984).
81. H. Coufal, J. Stöhr and K. Baberschke, in *Photoacoustic and Photothermal Phenomena* (P. Hess and J. Pelzl, Eds., Springer-Verlag, Heidelberg, 1988), p. 25.
82. T. Hinoue, S. Kawada, M. Murata and Y. Yokoyama, *Chem. Lett. (Jpn.)*, 2061 (1988).
83. K. Tanaka, K. Sindoh and A. Odajima, *Rep. Progr. Polym. Phys. Jpn.*, **29,** 367 (1986).
84. K. Tanaka, Y. Ichimura and K. Sindoh, *J. Appl. Phys.*, **63,** 1815 (1988).
85. F. Boucher and R. M. Leblanc, *Can. J. Spectrosc.*, **26,** 190 (1981).
86. A. Mandelis, R. Wagner, K. Ghandi, R. Baltman and P. Dao, *Phys. Rev.*, **B39,** 5254 (1989).
87. A. Mandelis, W. Lo and R. E. Wagner, *Appl. Phys.*, **A44,** 123 (1987).
88. R. K. Grygier, W. Knoll and H. Coufal, *Can. J. Phys.*, **64,** 1067 (1986).
89. S. Negm and H. Talaat, in *Photoacoustic and Photothermal Phenomena II*, (J. C. Murphy, J. W. Maclachlan Spicer, L. C. Aamodt and B. S. H. Royce, eds., Springer Ser. Opt. Sci., Vol. 62, Heidelberg, 1990), p. 120.
90. T. Inagaki, M. Motosuga, E. T. Arakawa and J. P. Goudonnet, *Phys. Rev.*, **B32,** 2548 (1985).
91. A. Mandelis, F. Boroumand, H. Solka, J. Highfield and H. van den Bergh, *Appl. Spectrosc.*, **44,** 132 (1990).
92. A. Mandelis, F. Boroumand and H. van den Bergh, *Spectrochimica Acta A* (in press).

93. C. Christofides and A. Mandelis, *J. Appl. Phys.*, **66,** 3975 (1989).
94. R. L. Melcher and G. V. Arbach, *Appl. Phys. Lett.*, **40,** 910 (1982).
95. J. A. Simpson and A. J. Tuzzolino, *Phys. Rev. Lett.*, **52,** 601 (1984).
96. V. M. Apatin and G. N. Makarov, *Appl. Phys. B* **28,** 367 (1982).
97. M. Faubel and S. Schlemmer, *J. Phys. E.*, **21,** 75 (1988).
98. P. E. Dyer and R. Srinivasan, *J. Appl. Phys.*, **66,** 2608 (1989).
99. H. Winters, H. Coufal, C. Rettner and D. Bethune, *Phys. Rev.*, **B,** in the press.